https://doi.org/10.5194/egusphere-2024-797
Preprint. Discussion started: 2 April 2024

Experimental investigation of the interplay between transverse mixing and pH reaction in porous media

Adi Biran[1], Tomer Sapar[1], Ludmila Abezgauz[1], and Yaniv Edery[1]

[1] Faculty of Civil and Environmental Engineering, Technion, Haifa, Israel.

Correspondence to: Yaniv Edery (yanivedery@technion.ac.il)

Abstract. pH-induced reactive transport in porous environments is a critical factor in Earth sciences, influencing a range of natural and anthropogenic processes such as mineral dissolution/precipitation, adsorption/desorption, microbial reactions, and redox transformations. These processes, pivotal in carbon capture and storage (CCS) applications to groundwater remediation, are determined by pH transport. However, the uncertainty in these macroscopic processes' stems from pore-scale heterogeneities and the high diffusion value of the ions and protons forming the pH range. While practical for field-scale applications, traditional macroscopic models often fail to accurately predict experimental and field results in reactive systems due to their inability to capture the details of pore-scale pH range.

This study investigates the interplay between transverse mixing and pH-driven reaction in porous media. It focuses on how porous structure and flow rate affect mixing and chemical reaction dynamics. Utilizing confocal microscopy, the research visualizes fluorescently labeled fluids, revealing variations in mixing patterns from diffusive in homogenous to shear-driven in heterogeneous media. However, pH-driven reactions show a different pattern, with a faster reaction rate, suggesting quicker pH equilibration between co-flowing fluids than predicted by transverse dispersion or diffusion. The study highlights the unique characteristics of pH change in water, which significantly influences reactive transport in porous media.

1 Introduction

The distribution of most chemical species in a porous environment is generally determined by both transport and biogeochemical reactions, as described by the term reactive transport(Holzbecher, 2005)·(Carrera et al., 2022). Reactive transport is involved in diverse processes(Steefel and MacQuarrie, 1996), either naturally or anthropogenically occurring, such as mineral dissolution and precipitation(Noiriel and Soulaine, 2021; Stolze et al., 2022; Goldberg-Yehuda et al., 2022), adsorption and desorption(Carrillo-González et al., 2006; Nützmann et al., 2005), microbial reactions(Stocks-Fischer et al., 1999; Thullner et al., 2005), and redox transformations(Thullner et al., 2005; Sposito, 2008). It is important for the understanding of numerous Earth Sciences problems ranging from engineering applications such as carbon capture and storage or groundwater remediation, as well as geological studies, to watershed or global issues(Carrera et al., 2022).

Reactive transport in porous media can be described with either pore-scale or Darcy-scale (macroscopic) models. Although pore-scale simulations have a solid physical foundation, they require knowledge of pore size distribution,

https://doi.org/10.5194/egusphere-2024-797
Preprint. Discussion started: 2 April 2024

geometry, tortuosity, and connectivity. These are seldom available and are impractical as predictive tools at scales that are orders of magnitude larger than the pore scale. Therefore, macroscopic models have developed to overcome these limitations(Battiato and Tartakovsky, 2011; Valocchi et al., 2019; Ghaderi Zefreh et al., 2019). Macroscopic representation is based on upscaling the porous medium by averaging it over space and time scales in a representative elementary volume (REV), which allows the replacement of a solid-liquid domain with an equivalent continuum(Chiogna and Bellin, 2013).

At the macroscale, the advection-dispersion reaction equation (ADRE) is usually used to describe reactive transport. However, it may provide incorrect predictions of experimental results in reactive systems, including the extent of reactions in mixing-controlled chemical transformations(Battiato and Tartakovsky, 2011; Berkowitz et al., 2016). This is mainly because the ADRE is not sensitive to incomplete mixing at the pore scale, in which biogeochemical reactions occur(Edery et al., 2013, 2009; Alhashmi et al., 2015).

Mixing is the process that brings reactants together, enabling them to ultimately react, and it is related to scale(Alhashmi et al., 2015; Acharya et al., 2007; Guadagnini et al., 2009; Dentz et al., 2011; Al-Khulaifi et al., 2017; Rücker, n.d.). The high degree of variability in pore-scale mixing impacts the larger-scale reactive transport behavior(Datta et al., 2013; Browne and Datta, 2023). Due to this mixing multiscale nature, there is still a lack of understanding of the integration between coupled transport and reactions at multiple scales of the porous medium, which possess a challenge in predicting mixing-driven reactions(Edery et al., 2015; Tartakovsky et al., 2009; Borgman et al., 2023). Thus, it is necessary to measure both mixing and reaction at the pore scale, regarding pore properties.

It is particularly essential to understand how mixing patterns at the pore scale affect pH-driven chemical reactions, as these reactions are ubiquitous in porous media, such as soils and aquifers(Lai et al., 2015). Examples of such reactions are dissolution and precipitation of soil carbonates and sulfates(Sposito, 2008), nitrification and denitrification processes(Ward et al., 2011; Edery et al., 2011, 2021; Shavelzon and Edery, 2023), protonation and deprotonation of carboxyl and phenolic groups in soil organic matter(Sparks et al., 2024). Soil pH has an enormous influence on soil biogeochemical processes, as it influences the solubility of plant nutrients, phytotoxic elements, and pollutants, and determines their biological availability and mobility(Penn and Camberato, 2019; Neina, 2019; Waisbord and Guasto, 2016).

This study focuses on investigating transverse incomplete mixing due to parallel flow field within a porous medium ranging from homogeneous to heterogeneous, and its effect on pH-driven reaction. This is done by visualizing fluorescently labeled fluids using a confocal microscope, for mixing and reaction. The experiments showed that transverse mixing varies from diffusive mixing in the homogeneous case to shear-driven mixing in the heterogeneous case. However, the pH-driven reaction does not follow this mixing pattern. Instead, it shows a faster reaction rate, which suggests that the pH difference between the co-flowing fluids equilibrates faster than the mixing, as the proton transfer mechanism is comparatively faster than the transverse dispersion or diffusion.

https://doi.org/10.5194/egusphere-2024-797
Preprint. Discussion started: 2 April 2024

2 Methods

To investigate how the porous structure and flow rate influence mixing and chemical reaction, three sets of experiments are employed to visualize mixing and reaction in a porous medium. The first set is mixing experiments, where a conservative tracer is used to test the effect of different pore size variations (heterogeneities) with different flow rates on the local mixing dynamics. In the second set a reactive experiment is employed under the same conditions as the conservative experiments, where the pH reactant is uniformly distributed at the flow cell, and only the pH is unevenly distributed. And in the third set, both the pH and pH reactant are unevenly distributed in the cell to examine the effect of mixing on neutralization reaction dynamics, resulting in pH change, under the same conditions.

2.1 Experimental setup

All sets of experiments, shown in Figure 1.a.-c., were performed in a Polydimethylsiloxane (PDMS) microfluidic flow cell, sized ~4.5 mm X 1.3 mm X 0.05 mm. Each cell was composed of ~300 cylindrical pillars ($R = 50\ \mu m$) so the internal porosity of the cell was ~60%. The tracer moved only in the pore space among the pillars, which were set in four different arrangements within the cell to achieve four different levels of heterogeneity: from completely homogeneous where the pillar center were set on a perfect lattice grid with normalized standard deviation of $\frac{\sigma}{R} = 0$, to the most heterogeneous arrangement where the pillars centers were randomly moved in the x and y direction following a Gaussian distribution with normalized standard deviation of $\frac{\sigma}{R} = 0.5$ (see Figure 1.d.).

Each cell had two parallel inlets (right and left), each of them set at 425 µm from the edge of the cell, and one funnel shaped outlet. The fluorescent conservative tracer used for the mixing experiments (Figure 1.a.) is rhodamine 6G (R6G), which is widely used to visualize flow patterns, such as in the domain of environmental hydraulics(Barzan and Hajiesmaeilbaigi, 2018). Pyranine (8-hydroxypyrene-1,3,6-trisulfonate) is used for the reactive and combined experiments (Figure 1.b.-c.), as its fluorescent emission spectra and intensity are highly dependent on medium pH(Avnir and Barenholz, 2005), therefore suitable for monitoring pH changes. The tracer's concentrations were 2 mg/50 ml double distilled water (DDW) for the R6G (corresponding to 0.083 mM) and 9 mg/50 ml DDW for the pyranine (corresponding to 0.347 mM).

pH values used for the reactive experiments were 7.3 and 12.3, resulting in higher and lower emission intensities, respectively. As such, they are related to their respected tracer and background solution. To achieve the wanted pH we added a strong acid or a strong base (hydrochloric acid and sodium hydroxide respectively), to the pyranine aqueous solutions.
When HCl is added it ionizes to form the hydronium ion:

$$HCl_{(aq)} + H_2O \leftrightarrow H_3O^+_{(aq)} + Cl^-_{(aq)} \quad (1)$$

When NaOH is added it ionizes to form the hydroxide ion:

$$NaOH_{(aq)} \leftrightarrow Na^+_{(aq)} + OH^-_{(aq)} \quad (2)$$

When set together, the hydronium and hydroxide ions react to form water in a neutralization reaction:

https://doi.org/10.5194/egusphere-2024-797
Preprint. Discussion started: 2 April 2024

$$H_3O^+_{(aq)} + OH^-_{(aq)} \leftrightarrow 2H_2O \quad (3)$$

While the pyranine ($ROH_{(aq)}$) reaction is mainly with the $OH^-_{(aq)}$ as the reactive experiment is performed under basic pH:

$$ROH_{(aq)} + OH^-_{(aq)} \leftrightarrow RO^-_{(aq)} + H_2O\,, \quad (4)$$

and, therefore, the intensity is mainly decreasing with the pH change (Figure 1.e.).

To perform the mixing and reactive experiments, we saturate the flow cell with the background solution, i.e., DDW for the mixing experiments, and pyranine solution at a pH of 12.3 for the reactive experiments. Subsequently, a 100 µl glass syringe, filled with the tracer, i.e., R6G or pyranine at pH of 7.3, is connected directly to the left inlet to reduce the experimental time until the tracer/pyranine reaches the cell and forms an interface with the background fluid.

A picture of the cell, filled with the background solution, is taken before the insertion of the conservative/reactive tracer, providing a base image for the image analysis calibration. Thereafter, both 100 µl syringes with the tracer/pyranine and background solution are placed in the same syringe pump with a pre-defined flow rate. This way, the background solution flowed from the right inlet, and the tracer flowed from the left inlet, having the same flowrate, while interfacing roughly in the middle of the cell.

Changes in color intensity of the conservative tracer occurred due to mixing (or dilution), while for the reactive tracer, they were due to a pH change followed by the neutralization reaction. Finally, the cell is saturated manually with the tracer itself (i.e., R6G for mixing experiments and pyranine at pH of 7.3 for reactive experiments) from both inlets, to produce a high-intensity, final image with known concentration for the image analysis calibration.

The third set of experiments combines both concentration gradient and pH gradient, using DDW at a pH of 12.3 as the background solution and pyranine at a pH of 7.3 as the reactive tracer. pH values were achieved using NaOH and HCl, similar to the reactive experiments. The combined experiments are made in the same process mentioned above, but only within the completely homogeneous medium and the most heterogeneous one, to present the effect of simoltenous migration

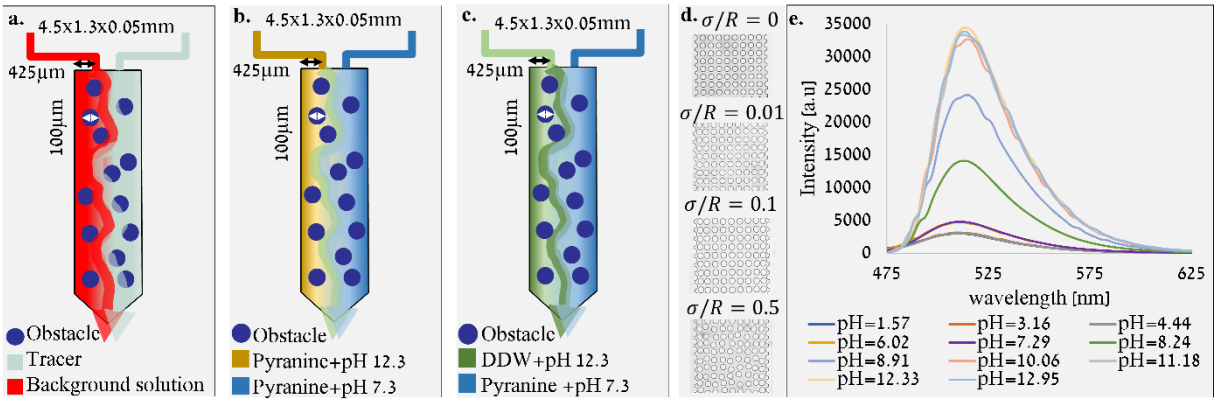

Figure 1: a. An illustration of the mixing experiment setup. b. An illustration of the reactive experiment setup (pH gradient only). c. An illustration of the combined experiment setup (pyranine concentration gradient and pH gradient). d. Four different pore size variations (heterogeneities) of the flow cell, from the homogeneous one (σ/R=0) to the most heterogeneous (σ/R=0.5). e. Intensity of pyranine emission versus wavelength for various pH, as measured by UV-vis, and verified under the confocal.

https://doi.org/10.5194/egusphere-2024-797
Preprint. Discussion started: 2 April 2024

of pyranine and pH.

2.2 Imaging

For both the tracer and reactive experiments, a confocal microscope was used to visualize mixing and reaction within the flow cell. The rhodamine 6G tracer is excited by a 546 nm laser, and tracked with the emission wavelength of 600 nm, while the pyranine is excited by a 405 nm laser and tracked with the emission wavelength of 550 nm. Images from the confocal are taken by a Prime BSI camera with a 95% quantum efficiency and 1e- median noise, with an exposure time of 500 msec, bit depth of 16-bit, and magnification of x2.

For the 100 µl/hr flow rate (Darcy velocity of $v_d = 0.142\frac{cm}{sec}$), a series of pictures were taken, for 5 minutes after forming a stable interface between the fluids. Then, after additional 5 minutes of delay, another series of pictures is taken, under the same conditions, to verify the stability of the interface. For the 10 µl/hr flow rate ($v_d = 0.0142\frac{cm}{sec}$), the same imaging sequence was performed, with a time difference of 10 minutes. For both flow rates, all the pixel intensity at pixel ij (I_{ij}) difference between the initial and later imaging sequence that exceeded the 0.1% (white noise of the camera) were averaged in absolute terms, and the stability of the interface was established if the average difference was isotropic and smaller than 1% (namely, $\langle\frac{|I_{ij}(t=5)-I_{ij}(t=10)|}{|I_{ij}(t=10)|} > 0.1\%\rangle < 1\%$), a similar analysis was performed around the interface to verify that the 1% difference is not the outcome of the bulk behaviour.

2.1 Image Analysis

A MATLAB image processing program is developed to convert the image intensity received in the mixing experiments to normalized tracer concentration. Similarly, a program is developed to convert the image intensity received in the reactive experiments to its pH values.

2.1.1 Mixing experiments

Conversion of image intensity to normalized tracer concentration is based on the Bear-Lambert law, dictating a linear relationship between the concentration and the absorbance of the solution(Barzan and Hajiesmaeilbaigi, 2018). The maximum and minimum intensity images are set to establish the scale between the maximum and minimum tracer concentration. The difference between each intermediate intensity and the minimal intensity is normalized to the difference between maximum and minimum intensities, yielding a unitless number between zero to one, i.e., the normalized tracer concentration:

$$C_{ij} = \frac{I_{ij} - I_{ij}(min)}{I_{ij}(max) - I_{ij}(min)}\ [-] \qquad (5)$$

https://doi.org/10.5194/egusphere-2024-797
Preprint. Discussion started: 2 April 2024

Recall that I_{ij} is the image intensity at pixel ij, $I_{ij}(min)$ is the intensity of the background solution image (DDW), and $I_{ij}(max)$ is the intensity of the tracer itself (not diluted) image. The validity of the method was verified for our setup as well as in other studies.(Barzan and Hajiesmaeilbaigi, 2018)

2.1.2 Reactive experiments

Unlike the tracer experiment, the intensity change of the pyranine due to the pH does not scale linearly, thus, a scheme of the process of converting raw data to pH distribution is developed for this study (shown in Figure 2). For the conversion of image intensity to pH it was necessary to find a correlation between the two. To create a calibration curve, samples of pyranine dissolved in DDW (0.347 mM as in the experiments) at different pH values were made using HCl and NaOH. The flow cell was manually saturated with a certain sample, and an image of the cell was taken. The mean intensity of each image was then calculated.

The correlation between pH and mean image intensity was fitted (MATLAB Curve Fitting Tool application), in which a descending exponential function was set to fit the received calibration curve ($R^2 = 0.976$), shown in Figure 2.b. The equation is as follows:

$$y = -e^{a \cdot x} + b \qquad (6)$$

where y corresponds to the image mean intensity, x corresponds to the pH value, while a establishes the decedent rate ($a = 0.4977$), and b is the maximum intensity ($b = 935.7$), and both are fitting parameters. This rapid exponential change in

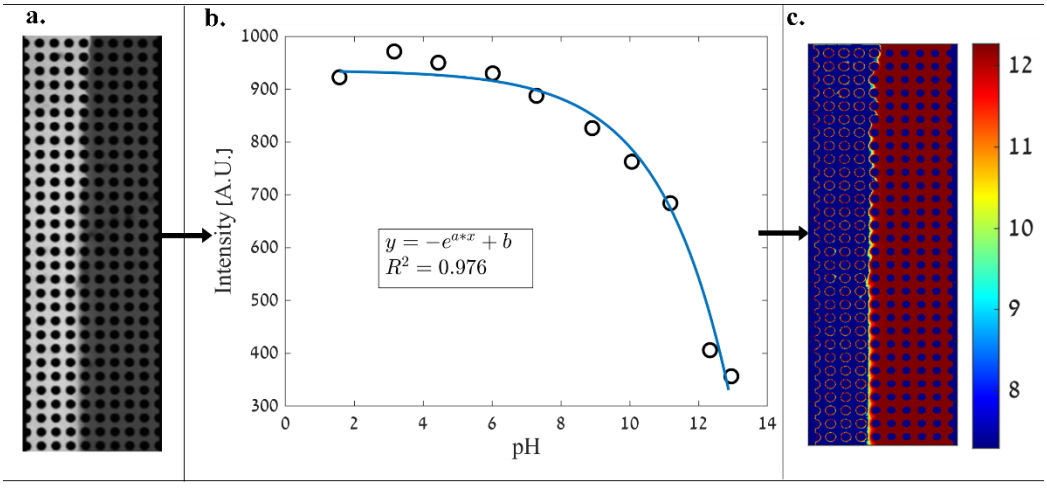

Figure 2: Scheme of the process of converting image intensity to pH distribution. a. Raw image, showing the intensity of pyranine (0.347 mM) at pH of 7.3 on the left and at pH of 12.3 on the right. b. Calibration curve showing mean intensity of pyranine (0.347 mM) at different pH values, excited at 405 nm, as measured within the flow cell. c. Analyzed data image, showing pH distribution.

intensity due to pH marks the sensitivity of the pyranine to a narrow range of pH, which is reflected in the sharp transition

https://doi.org/10.5194/egusphere-2024-797
Preprint. Discussion started: 2 April 2024

between the pH values in Figure 2.c., and the following experimental pH results. The consumption of OH^- by the pyranine will be negligeble in changing the overall pH as the pyranine concentration in equilibrium with the ions.

For the image analysis, we first fit a specific value of each of the parameters a and b in equation (6) to the intensity of each pixel composing the image. This is done by the two images produced at the beginning and the termination of each experiment, by cell saturation with pyranine solution at pH of 12.3 and 7.3, respectively. Using image intensities of these two known pH values and equation (6), we find a and b matrices for each separate experiment, and for each pixel, which are subsequently used for the conversion of image intensity to pH.

In both the intensity data and the analyzed pH image, there is a noticeable transition of the interface from left to right, or from high pH to low pH. This transition is due to the diffusive nature of the OH^-ions from their higher concentration to their lower concentration. This shift in the interface was reported in previous studies, leading to the shift in precipitation of $CaCO_3$.(Katz et al., 2011; Tartakovsky et al., 2008, 2007) As such, observing this shift in our experimental setup is in line with previous studies on pH induced reactions.

3 Results and Discussions

The results start in presenting the tracer experiments, showing how the heterogeneity level leads to various transverse mixing (section 3.1), followed by a calculation of the predicted pH by the measured mixing, and subsequently comparing this calculated pH with the measured pH experiments (section 3.2). The experimental part is concluded by the presentation of the combined experiments (section 3.3). In the Supplementary we also present the results of the COMSOL simulations performed for the tracer, and reactive experiments, which narrates the significance of considering the different diffusion rates for the reactant components, and the role of pH in the mixing process.

3.1 Mixing experiments

As the tracer is inserted into the left side of the flow cell with a given flow rate, while the right side experiences the same flow rate only without the tracer, we observe tracer migration between the sides due to the concentration gradient, via diffusion and transverse dispersion. The maximum normalized tracer concentration ($C_{ij} = 1$) is indeed at the left side, while the right side is at its minimum ($C_{ij} = 0$), as shown in Figure 3.1. Yet, the transition between the concentrations, representing the mixing due to diffusion and dispersion, varies according to the heterogeneity of the medium.

Both homogeneous and heterogeneous media show a relatively sharp change in the tracer mixing at the interface on the upper volume of the cell up-flow; this interface gradually increases down-flow as the diffusion and dispersion propagate and drive the mixing between the fluids. However, this mixing mechanism, captured by the interface increase, varies in size and character from the homogeneous medium (Figure 3.1.a. and e.) to the most heterogeneous one (Figure 3.1.d. and h.). While in the homogeneous media, mixing is symmetrical within the cell, in the heterogeneous medium mixing is determined by the pillars setting and moves between different pores.

https://doi.org/10.5194/egusphere-2024-797
Preprint. Discussion started: 2 April 2024

This change in mixing pattern demonstrates the different mechanisms governing the mixing as affected by the variations in pore size: mixing in the homogeneous medium is controlled mainly by diffusion, as shear forces effects are negligible, while in the heterogeneous medium, where pore size varies forming tortoise route among pillars, mixing is dominated by shear forces acting on the fluid close to the obstacle's boundaries. These forces result from the velocity gradient created due to the different pore sizes, where the smaller pores result in lower velocities and higher shear forces.

The relation between the two described mechanisms (shear forces vs. diffusion) is reflected in the Peclet number (Pe):

$$Pe = \frac{v_d R}{D} \quad (7)$$

which is a measure of the velocity magnitude (v_d), which approximate the shear forces, and the diffusion (D), which is an intrinsic property of the fluids over the mean pore size (R)(Bossis and Brady, 1987). While the Pe numbers are low, they

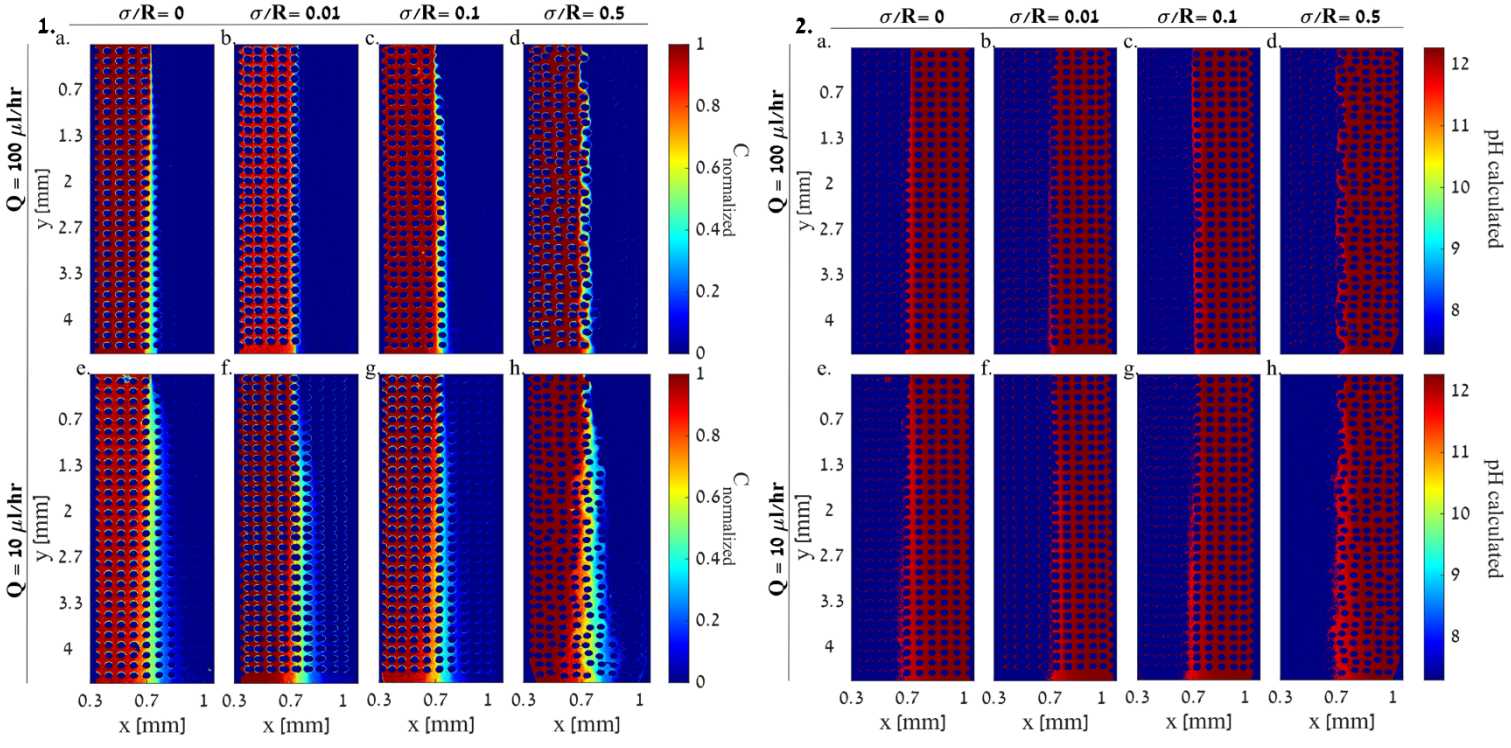

Figure 3: Mixing experiments depicting the distribution of the conservative tracer normalized concentration for: 1. a.-d. flow rate of 100 µl/hr at medium heterogeneities of σ/R=0, σ/R =0.01, σ/R =0.1 and σ/R =0.5, respectively; and 1.e.-h. flow rate of 10 µl/hr at medium heterogeneities of σ/R=0, σ/R =0.01, σ/R =0.1 and σ/R =0.5, respectively. And predicted pH calculated from the normalized tracer concentration received in the mixing experiments for: 2. a.-d. flow rate of 100 µl/hr at medium heterogeneities of σ/R =0, σ/R =0.01, σ/R =0.1 and σ/R =0.5, respectively; and 2. e.-h. flow rate of 10 µl/hr at medium heterogeneities of σ/R=0, σ/R =0.01, σ/R =0.1 and σ/R =0.5, respectively.

still indicate that the velocity magnitude has dominance on the diffusion in the pore scale (see table 1), known to be critical in reactive transport(Nissan and Berkowitz, 2019). Mixing experiments results of the 10 µl/hr flow rate (Figure 3.1.e.-h.)

https://doi.org/10.5194/egusphere-2024-797
Preprint. Discussion started: 2 April 2024

show that in all medium heterogeneities, the interface between tracer and DDW is wider compared to the 100 µl/hr flow rate, demonstrating the larger effect of diffusion as the flow rate descends.

Comparing heterogeneities of σ/R=0, σ/R =0.01, and σ/R =0.1 (Figure 3.1.e.-g.), we see the more significant effect of diffusion in the homogeneous and nearly homogeneous medium, as mixing is received closer to the inlets. The most heterogeneous medium (Figure 3.1.h.) also shows a more dispersive pattern that encompasses several pore lengths, and points to the more dominant role of shear over the diffusion.

Assuming the reaction follows the mixing pattern, which is controlled by the tracer dispersion and diffusion rate through water molecules, we calculate the predicted pH according to the normalized tracer concentration received in the mixing experiments, as shown in Figure 3.2. As the pyranine changes with the OH^-groups, we base the calculation of pH on the OH^-migration. This is done by the equation below:

$$pH_{calculated} = -(14 - log[C_{ij} \cdot 10^{-(14-low\ pH)} + (1 - C_{ij}) \cdot 10^{-(14-high\ pH)}]) \quad (8)$$

where $low\ pH$ and $high\ pH$ are the pH values of the reactive tracer solutions, i.e., 7.3 and 12.3, respectively.

3.2 Reactive experiments

Similarly to the mixing experiments, and following the experimental procedure described, we performed reactive experiments with flow rates of 100 µl/hr (Figure 4.a.-d.) and 10 µl/hr (Figure 4.e.-h.). The mixing experiments provide the distinction between the role of diffusion and shear forces, where the first is manifested in the homogeneous, low-velocity case, and the latter is apparent in the heterogeneous and high-velocity case. This tendency is also demonstrated in the distribution of the pH calculated according to the normalized tracer concentration, received from the mixing experiments. However, the reactive experiments show that the reaction pattern does not necessarily follow the mixing pattern, particularly as the medium becomes more heterogeneous and the flow rate descends.

Of all the tested conditions, the patterns received in the homogeneous and the slightly heterogenous (σ/R = 0 and 0.01, respectively) media at a flow rate of 100 µl/hr in the reactive experiments (Figure 4.a.-b.) and the pH predicted by the mixing (Figure 3.2.a.-b.), are relatively similar. In these conditions, the interface is almost symmetrical within the cell, although we do see a sharper gradient when the reaction occurs and a narrower interface, probably due to the pyranine intensity exponential decay (Figure 2).

Examining the reaction pattern at a flow rate of 100 µl/hr in the more heterogeneous media, i.e., σ/R =0.1 and 0.5 (Figure 4.c.-d.), clearly shows that the interface between the two fluids is not received in the middle of the cell. Rather, it tends to migrate leftwards as the flow proceeds, indicating that the reaction occurs earlier and closer to the area of the lowest pH (7.3). This interface migration due to the diffusive nature of the OH^-ions from high to low concentration occurs for all medium heterogeneities, and was reported in previous studies on precipitation of $CaCO_3$,(Katz et al., 2011; Tartakovsky et al., 2008, 2007) yet it becomes more dominant as the medium is more heterogeneous.

https://doi.org/10.5194/egusphere-2024-797
Preprint. Discussion started: 2 April 2024

At a lower flow rate, narrower interfaces are received in the reactive experiments than those predicted by the mixing, at all medium heterogeneities (Figure 4.e.-h. and Figure 3.2.e.-h., respectively). As seen in the 100 µl/hr flow rate, this
230 tendency is more noticeable as the medium becomes more heterogeneous. However, as heterogeneity increases, it appears that reaction tends to occur earlier at the lower flow rate as the flow proceeds. This is demonstrated in Figure 4.c.-d. comparing to Figure 4.g.-h., where the last present a sharper migration of the interface so that a larger volume of the cell

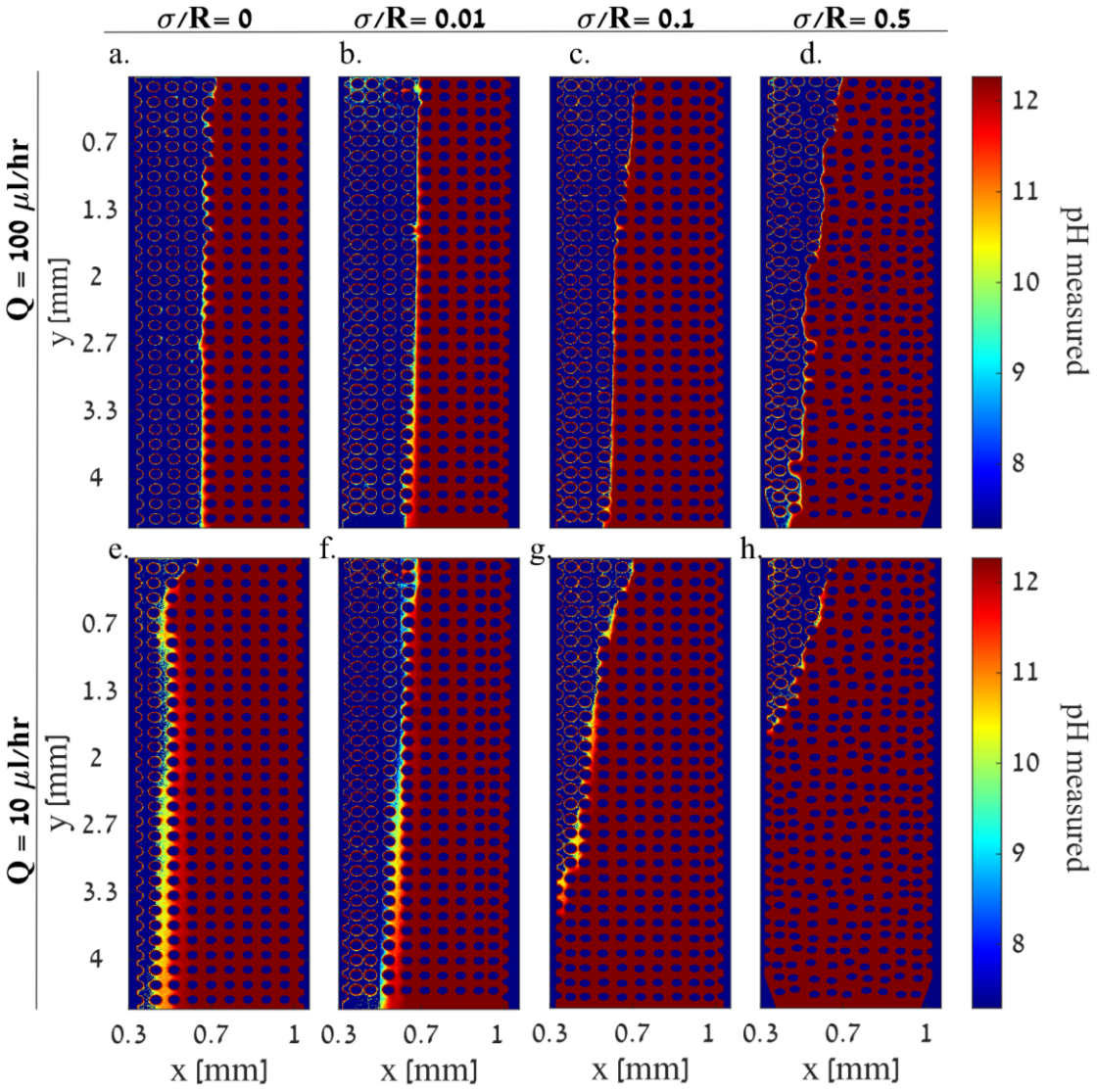

Figure 4: Reactive experiments: pH values as indicated by the reactive tracer distribution. a.-d. Flow rate of 100 µl/hr at medium heterogeneities of σ/R=0, σ/R =0.01, σ/R =0.1 and σ/R =0.5, respectively. e.-h. Flow rate of 10 µl/hr at medium heterogeneities of σ/R =0, σ/R =0.01, σ/R =0.1 and σ/R =0.5, respectively.

https://doi.org/10.5194/egusphere-2024-797
Preprint. Discussion started: 2 April 2024

indicates high pH.

As predicted by the mixing experiments, the calculated pH at 10 µl/hr flow rate (Figure 3.2.e.-h.) also shows asymmetrical patterns regarding the highest vs. lowest pH distribution (12.3 to 7.3, respectively). Moreover, mixing predicts a narrower strip of the highest pH as fluids move towards the outlet zone as the interface, in which the reaction theoretically occurs, gets larger due to tracer diffusion. But reactive experiments show that as fluids move vertically along the cell, the volume of the highest pH is increased on account of the lowest pH. This increase is the outcome of the logarithmic scale of pH, where molar value of the access OH^- ion are orders of magnitude higher on one side, which dominate over the cross-section. This demonstrates that the reaction does not necessarily follow the mixing pattern in porous media, as the pH gradient equilibrates faster than the tracer concentration gradient.

3.2.1 The role of diffusion in pH transverse migration

While the logarithmically high OH^- concentration explains the one sided migration, the rate of migration follows the high proton mobility in water(Agmon, 1995). It has already been well established that proton transfers are one of the fastest chemical processes and even in diluted solution phase, when diffusion is limited, their rates exceed other known reactions(Donten et al., 2012). This is usually explained in terms of a sequence of proton-transfer reactions between water molecules along a hydrogen-bonded network, known as proton hops, as described in the Grotthuss mechanism ~200 years ago(Agmon, 1995; Hassanali et al., 2011; Wolke et al., 2016). Due to its tiny ionic radius and its strong polarization power, the proton cannot be isolated in equilibrium conditions. Instead, it immediately binds to an intact water molecule to form hydronium ions by creating covalent bonds(Thabet et al., 2020).

The Grotthuss mechanism was proposed to explain how the excess proton occurring as hydronium ion diffuses much faster than expected from its hydrodynamic radius. In this mechanism, the excess proton diffuses with a proton transfer from the hydronium to the neighboring water molecule, or from a water molecule to a neighboring hydroxide(Hassanali et al., 2011; Chen et al., n.d.).

The differences between the proton/hydronium diffusion rate to the tracer diffusion rate are reflected in their diffusion coefficients in water, as the former is more than one order of magnitude larger than the latter, with a diffusion coefficient (D) of $9.3 \cdot 10^{-5} \frac{\mathrm{cm}^2}{\mathrm{s}}$ (Amdursky et al., 2019; Zhang et al., 2021; Tuckerman et al., 2006) for hydronium vs. $4 \cdot 10^{-6} \frac{\mathrm{cm}^2}{\mathrm{s}}$ (Gendron et al., 2008) for R6G, and close to one order for the OH^-, shown in table 1.

This high diffusion rate leads to a diffusion dominated transvers flux captured by the low Pe over the pore size. Calculating the OH^- transverse migration over the ~10 sec it takes for the fluid to advance 1.3 mm for the 10 µl/hr flow rate (recall that the $v_d = 0.0142 \frac{cm}{sec}$), the high diffusion advances the OH^- only 0.228 mm. As diffusion is symmetrical in nature, it is not only occurring transversely to the flow but also aligned with the flow, leading to a steady state of OH^- neutralized by the lower pH, as seen in the homogeneous case (Figure 4. e). However, for the same extent of time and Darcy velocity, the high shear in the heterogenous case further mixes the OH^-, leading to full homogenization of the pH in the flow cell

https://doi.org/10.5194/egusphere-2024-797
Preprint. Discussion started: 2 April 2024

(Figure 4.h). Yet, the same increase in shear between the homogeneous and the heterogenous case for the high flux\Pe, produces a smaller relative effect on the OH^- migration (Figure 4. a-d).

3.2.2 Comparing the average pH transverse migration

Most studies and experiments do not have access to the pH or tracer spatial distribution, and therefore they relay on measuring the average values of pH in the system at a given volume. To reproduce this measurement, we further compare the averaged pH distribution received in the reactive experiments with the averaged theoretical one we calculated according to the conservative tracer concentration. Using a MATLAB program, we divided each analyzed image (of Figure 3.2 and Figure 4) into three, size-equal sections: inlet area, middle area, and outlet area (see Figure 5.2.). In each section, we calculated the average pH of each column of the matrix along the x-axis. The plotted results, shown in Figure 5.1.a.-h., emphasize that the tendencies we mentioned before persist even when averaged spatially.

Mixing predicts that the average pH of the first section of the medium (red continuous line) starts to rise roughly in the middle of the cell. As we look at areas closer to the cell outlet, the average calculated pH (red dashed and dotted lines) starts to rise farther from the middle of the cell. However, the average pH measured in the reaction shows an opposite tendency- the farther away from the cell inlet, the sooner the pH rises along the x-axis.

Moreover, mixing predicts a more moderate climb of the average pH as the flow rate descends from 100 µl/hr to 10 µl/hr, which we do see in the reaction in practice, particularly in the inlet area (blue continuous lines in Figure 5.1.a. vs e., b. vs f., c. vs g. and d. vs h.). However, at the lower flow rate, the increase in pH starts significantly earlier in all the tested heterogeneities. This reflects the differences of diffusion time between the high to the low fluxes discussed earlier, as we saw

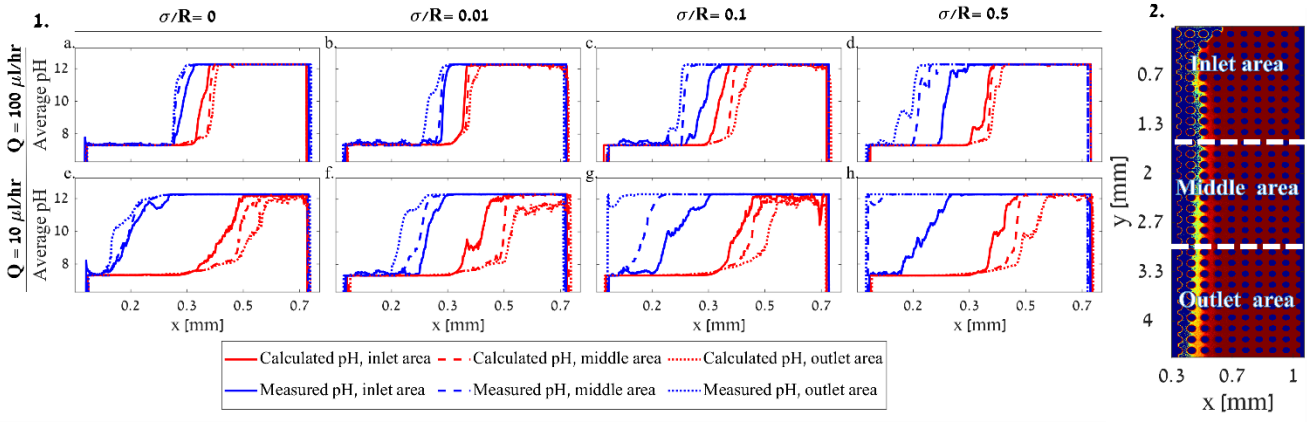

Figure 5: 1. a.-h. Average pH along the x-axis at three different sections of the flow cell: inlet area (continuous line), middle area (dashed line), and outlet area (dotted line), as calculated by the tracer concentration received in the mixing (red line) and as measured in the reaction (blue line). 1. a.-d. Flow rate of 100 µl/hr at medium heterogeneities of σ/R=0, σ/R =0.01, σ/R =0.1 and σ/R =0.5, respectively; and 1. e.-h. Flow rate of 10 µl/hr at medium heterogeneities of σ/R=0, σ/R =0.01, σ/R =0.1 and σ/R =0.5, respectively. 2.. An illustration of the flow cell division to three, size-equal sections.

in the mixing experiments where transverse diffusion dominates.

https://doi.org/10.5194/egusphere-2024-797
Preprint. Discussion started: 2 April 2024

The diffusion dominance is especially apparent in the sharp pH homogenization in the low flux, yet heterogeneity continues to play a role even in this low flux. The effect of heterogeneity on pH homogenization is reflected in the rapid transition of the middle cell pH as the heterogeneity level increases, and with it the shear forces increase. So overall, although the neutralization reaction occurs faster than the tracer concentration gradient equilibrium, it appears to be affected by both the fluids flow rate and medium heterogeneity in a similar manner to the tracer.

3.2.3 Calculating the ion concentration contribution to transverse migration

While the enhanced diffusion due to the Grotthuss mechanism is well established, the ionic nature of the proton/hydronium has the potential to form an electrical gradient that may affect the pH distribution. The contribution of this mechanism has been debated in the literature in the context of pH reaction, and shown that it can be neglected for brine, where the ion ratio is minor compared to the background solution (Li et al., 2006; Lichtner and Kang, 2007; Li et al., 2007) , yet it remains to be seen how relevant it is to the system presented in this study.

Following the Nernst-Planck equation(Bockris et al., 2006), the flux of ions due to both diffusion and migration under an electric field is given by:

$$J = -D_{OH^-}\frac{dC_{OH^-}}{dx} + u_{OH^-}C_{OH^-}\cdot E = = -D_{OH^-}\frac{\Delta C_{OH^-}}{\Delta x} + u_{OH^-}C_{OH^-}\cdot E \qquad (8)$$

where $J\ [\frac{\mathrm{mol}}{\mathrm{cm}^2}\cdot \mathrm{s}]$ is the flux of the ion, $C_{OH^-}\ [\frac{\mathrm{mol}}{\mathrm{cm}^3}]$ is the concentration of the ion, u is the ionic mobility, and E is the electric field. For the OH^-, the $D_{OH^-} = 5.3\times10^{-5}[\frac{\mathrm{cm}^2}{\mathrm{s}}]$, the $u_{OH^-} \approx 20\,\mathrm{x}\,10^{-8}\ [\frac{\mathrm{cm}^2}{V\cdot\mathrm{s}}]$ (see table 1 for details and reference), and knowing the concentration at both inlets and their distance ($\Delta x = 0.0475\ cm$), the $E \approx -2.5693\ [\frac{\mathrm{V}}{cm}]$.

We repeated this calculation for the hydroxide ions (OH^-), the protons (H^+), the Cl^- and the Na^+, and for all cases, the diffusive flux ($J_D(OH^-) \approx -5.35\times\ 10^{-5}$) was two to three orders of magnitude greater than the electric flux due to the ion concentration ($J_E(OH^-) \approx 2\times\ 10^{-7}$), making them negligible for our study (Bard and Faulkner, 2001).

Table 1. Mapping of the various chemical components in our system with their corresponding diffusion, ionic mobility, and Peclet value for both experimental fluxes. Details can be found in: (1) (Parkhurst and Appelo, 2013), (2) (Varcoe et al., 2014), (3) (Himmelsbach et al., 1998), and (4) (Gendron et al., 2008)

Chemical species	Diffusion [cm^2/s]	Ionic mobility [cm^2/sV]	Pe [$100/10\ \mu l/hr$]
H^+	9.31×10^{-5} (1)	36.2×10^{-5} (2)	7.6/0.76
OH^-	5.27×10^{-5} (1)	20.6×10^{-5} (2)	13.7/1.3

https://doi.org/10.5194/egusphere-2024-797
Preprint. Discussion started: 2 April 2024

Cl^-	2.01×10^{-5} (1)	7.91×10^{-5} (2)	35/3.5
Na^+	1.33×10^{-5} (1)	5.2×10^{-5} (2)	53/5.3
Pyranine	1.5×10^{-5} (3)		47/4.7
R6G	0.4×10^{-5} (4)		178/17

3.3 Combined experiments

In this study, we identify this neutralization reaction effect by setting fluids with the same reactive tracer concentration, so a concentration gradient is not present for the pyranine only the pH gradient. To mimic the practice where pH indicators are locally introduced and allowed to diffuse according to their concentration gradient and flow, we perform combined experiments where the pyranine is introduced only with the high pH inlet, and it will need to migrate towards the low pH area. The conversion of image intensity to pH is performed as made in the experiments involving pH gradient only, which is detailed in section 2.3.2. In this setup the pyranine dispersion is the limiting reactant for the pH reaction, and as such, the role it has as a pH indicator is limited, as its dilution acts as the limiting fluorescing factor, as shown in Figure 6.

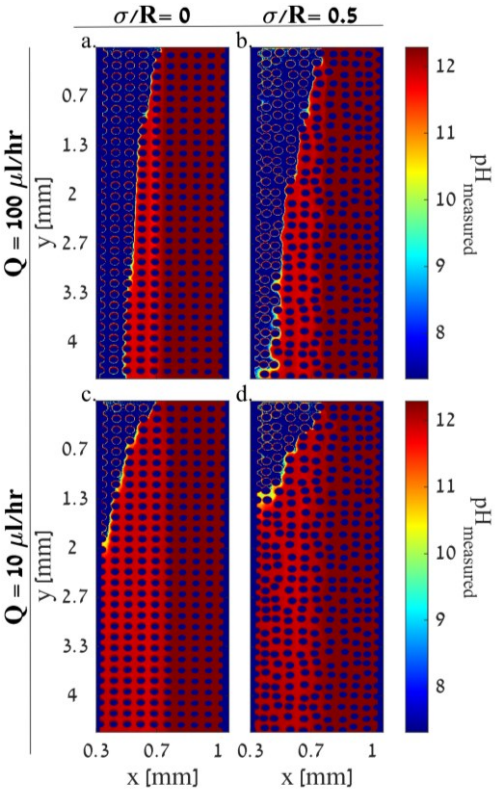

Figure 6: combined experiments (both concentration gradient and pH gradient): pH values as indicated by the reactive tracer distribution, neglecting tracer concentration gradient. a.-b. Flow rate of 100 µl/hr at medium heterogeneities of σ/R =0 and σ/R =0.5, respectively. c.-d. Flow rate of 10 µl/hr at medium heterogeneities of σ/R =0 and σ/R =0.5, respectively.

Although we should expect the same pH distribution within the porous media as for the tracer test, given that the pyranine diffusion is between the R6G and the OH^- value (see table 1), the image analysis yields a different distribution than the one accepted for the tracer or the pH (Figure 3.1.a. and e., and Figure 4.d. and h.). While the pH change is only due to the occurring reaction, here it is also wrongly accepted as a measure of the pyranine's transverse diffusion/dispersion, leading to the pyranine dilution which can be wrongly accounted as the pH change. This is reflected in the measured pH of ~11.5 phase we see in Figure 6.a.-d., which does not appear when the tracer's concentration gradient is not present in Figure 4. The interface between the phases of pH ~11.5 and pH=12.3 resembles the mixing pattern we get in the mixing experiments.

Another interesting aspect is the fast migration of pyranine, which cannot be accounted for by pyranine diffusion. Calculating the transverse diffusion for the pyranine in the form of mean square displacement presents higher pH homogenization for the homogeneous case, than the case where pyranine concentration is uniform in the cell, raising the

https://doi.org/10.5194/egusphere-2024-797
Preprint. Discussion started: 2 April 2024

question on if the OH^- concentration difference is facilitating migration in the form of osmotic pressure, while fixing the pyranine excitation levels.

4 Summary and Conclusion

We experimentally investigated the effect of porous media heterogeneity and flow rate on transverse mixing and their effect on the pH-driven neutralization reaction. The experiments showed that transverse mixing is controlled either by diffusion or by shear forces, while the former corresponds to the homogeneous medium and lower flow rate, and the latter corresponds to the heterogenous medium and higher flow rate. However, the pH reaction does not necessarily follow those mixing trends as the medium becomes more heterogeneous and the flow rate descends.

The pH gradient between the co-flowing fluids tends to equilibrate faster than the concentration gradient, so the reaction occurs earlier than predicted by the mixing pattern. The experiments demonstrate that a transition of a proton is considerably faster than diffusion and shear forces governing mixing. This can be accounted for by several mechanisms, resulting in the abnormally high proton mobility in water, known as the Grotthuss mechanism. The experiments presented here show how important it is to consider when incorporating pH-driven reactions in porous media. Even so, diffusion alone is not sufficient when considering neutralization reactions like pH, as is clear from the mismatch between the COMSOL simulations and the experimental results presented in the Supplementary of this paper.

This difference in diffusion rate can be easily missed as in most experimental setups, and in the field, pH is generally measured locally or with a pH indicator that migrates with the flow. The pH may equilibrate faster than the pH indicator diffusion due to the hydronium ions binding transition that does not require movement of the ion only dissociation of the water, while the pH indicator, and/or reactants, should distribute slower in the porous media as they lack this mechanism. Moreover, to avoid the charged balance calculation between the various ions and cations in the reactive system, with their respective diffusion coefficients (table 1), studies often assume that the diffusion is uniform for all chemical species. This assumption may hold while the background salinity is high (namely, close to sea water), yet for low salinity water this assumption becomes questionable. (Lichtner, 1996; Li et al., 2007; Lichtner and Kang, 2007)

As pH reactions are the most frequent and abundant reactions in soil and rock formation, considering the differences between pH migration and mixing is crucial to capturing the extent of reactions. Our findings raise questions on the assumption that the diffusion differences between reactants, specifically for pH reactions but also for various reactants as evident from the difference of transverse migration of the R6G and pyranine, are negligible. This assumption may be valid for higher Peclet, or for specific reactants, yet as typical flows in soil and rock generally follow low Peclet and involve pH reactions and\or rich ion composition, this assumption is rarely true.

Code and data availability. Code and data are available on a dedicated GitHub repository upon request to Yaniv Edery (yanivedery@technion.ac.il).

https://doi.org/10.5194/egusphere-2024-797
Preprint. Discussion started: 2 April 2024

Author contributions. AB developed the experimental methodology and performed all the experiments, analyzed data, and wrote major parts of the paper. TS developed the simulation code and performed numerical simulations. LA helped develop the experimental methodology. YE helped develop the experimental methodology, supervised and guided the experiments and simulations, and wrote major parts of the paper.

Competing interests. The contact author has declared that neither of the authors has any competing interests.

Financial support. This research has been supported by the German-Israeli Foundation (grant no. I-2536-306.8), and the Israel Science Foundation (grant no. 801/20).

Acknowledgments. YE and AB thank the German-Israeli Foundation (grant no. I-2536-306.8). YE, TB, and LA thank the Israel Science Foundation (grant no. 801/20).

References

Acharya, R. C., Valocchi, A. J., Werth, C. J., and Willingham, T. W.: Pore-scale simulation of dispersion and reaction along a transverse mixing zone in two-dimensional porous media, Water Resources Research, 43, https://doi.org/10.1029/2007WR005969, 2007.

Agmon, N.: The Grotthuss mechanism, Chemical Physics Letters, 244, 456–462, https://doi.org/10.1016/0009-2614(95)00905-J, 1995.

Alhashmi, Z., Blunt, M. J., and Bijeljic, B.: Predictions of dynamic changes in reaction rates as a consequence of incomplete mixing using pore scale reactive transport modeling on images of porous media, Journal of Contaminant Hydrology, 179, 171–181, https://doi.org/10.1016/j.jconhyd.2015.06.004, 2015.

Al-Khulaifi, Y., Lin, Q., Blunt, M. J., and Bijeljic, B.: Reaction Rates in Chemically Heterogeneous Rock: Coupled Impact of Structure and Flow Properties Studied by X-ray Microtomography, Environmental Science & Technology, 51(7), 4108–4116, https://doi.org/10.1021/acs.est.6b06224, 2017.

Amdursky, N., Lin, Y., Aho, N., and Groenhof, G.: Exploring fast proton transfer events associated with lateral proton diffusion on the surface of membranes, Proceedings of the National Academy of Sciences, 116, 2443–2451, https://doi.org/10.1073/pnas.1812351116, 2019.

Avnir, Y. and Barenholz, Y.: pH determination by pyranine: Medium-related artifacts and their correction, Analytical Biochemistry, 347, 34–41, https://doi.org/10.1016/j.ab.2005.09.026, 2005.

Bard, A. J. and Faulkner, L. R.: Fundamentals and applications, Electrochem Methods, 2, 482, 2001.

Barzan, M. and Hajiesmaeilbaigi, F.: Investigation the concentration effect on the absorption and fluorescence properties of Rhodamine 6G dye, Optik, 159, 157–161, https://doi.org/10.1016/j.ijleo.2018.01.075, 2018.

https://doi.org/10.5194/egusphere-2024-797
Preprint. Discussion started: 2 April 2024

Battiato, I. and Tartakovsky, D. M.: Applicability regimes for macroscopic models of reactive transport in porous media, Journal of Contaminant Hydrology, 120–121, 18–26, https://doi.org/10.1016/j.jconhyd.2010.05.005, 2011.

Berkowitz, B., Dror, I., Hansen, S. K., and Scher, H.: Measurements and models of reactive transport in geological media, Reviews of Geophysics, 54, 930–986, https://doi.org/10.1002/2016RG000524, 2016.

Bockris, J. O., Reddy, A. K., and Gamboa-Adelco, M. E.: Modern Electrochemistry 1, 2A, and 2B, Springer, 2006.

Borgman, O., Gomez, F., Borgne, T. L., and Méheust, Y.: Impact of structural heterogeneity on solute transport and mixing in unsaturated porous media: An experimental study, Copernicus Meetings, https://doi.org/10.5194/egusphere-egu23-11028, 2023.

Bossis, G. and Brady, J. F.: Self-diffusion of Brownian particles in concentrated suspensions under shear, The Journal of Chemical Physics, 87, 5437–5448, https://doi.org/10.1063/1.453708, 1987.

Browne, C. A. and Datta, S. S.: Harnessing elastic instabilities for enhanced mixing and reaction kinetics in porous media, https://doi.org/10.48550/arXiv.2311.07431, 13 November 2023.

Carrera, J., Saaltink, M. W., Soler-Sagarra, J., Wang, J., and Valhondo, C.: Reactive Transport: A Review of Basic Concepts with Emphasis on Biochemical Processes, Energies, 15, 925, https://doi.org/10.3390/en15030925, 2022.

Carrillo-González, R., Šimůnek, J., Sauvé, S., and Adriano, D.: Mechanisms and Pathways of Trace Element Mobility in Soils, in: Advances in Agronomy, vol. 91, Academic Press, 111–178, https://doi.org/10.1016/S0065-2113(06)91003-7, 2006.

Chen, M., Zheng, L., Santra, B., Ko, H.-Y., Jr, R. A. D., Car, R., and Wu, X.: Why does hydronium diffuse faster than hydroxide in liquid water?, n.d.

Chiogna, G. and Bellin, A.: Analytical solution for reactive solute transport considering incomplete mixing within a reference elementary volume, Water Resources Research, 49, 2589–2600, https://doi.org/10.1002/wrcr.20200, 2013.

Datta, S. S., Chiang, H., Ramakrishnan, T. S., and Weitz, D. A.: Spatial Fluctuations of Fluid Velocities in Flow through a Three-Dimensional Porous Medium, Phys. Rev. Lett., 111, 064501, https://doi.org/10.1103/PhysRevLett.111.064501, 2013.

Dentz, M., Le Borgne, T., Englert, A., and Bijeljic, B.: Mixing, spreading and reaction in heterogeneous media: A brief review, Journal of contaminant hydrology, 120, 1–17, 2011.

Donten, M. L., VandeVondele, J., and Hamm, P.: Speed Limits for Acid–Base Chemistry in Aqueous Solutions, Chimia, 66, 182, https://doi.org/10.2533/chimia.2012.182, 2012.

Edery, Y., Scher, H., and Berkowitz, B.: Modeling bimolecular reactions and transport in porous media, Geophysical Research Letters, 36, https://doi.org/10.1029/2008GL036381, 2009.

Edery, Y., Scher, H., and Berkowitz, B.: Dissolution and precipitation dynamics during dedolomitization, Water Resources Research, 47, https://doi.org/10.1029/2011WR010551, 2011.

Edery, Y., Guadagnini, A., Scher, H., and Berkowitz, B.: Reactive transport in disordered media: Role of fluctuations in interpretation of laboratory experiments, Advances in Water Resources, 51, 86–103, https://doi.org/10.1016/j.advwatres.2011.12.008, 2013.

https://doi.org/10.5194/egusphere-2024-797
Preprint. Discussion started: 2 April 2024

Edery, Y., Dror, I., Scher, H., and Berkowitz, B.: Anomalous reactive transport in porous media: Experiments and modeling, Phys. Rev. E, 91, 052130, https://doi.org/10.1103/PhysRevE.91.052130, 2015.

Edery, Y., Stolar, M., Porta, G., and Guadagnini, A.: Feedback mechanisms between precipitation and dissolution reactions across randomly heterogeneous conductivity fields, Hydrol. Earth Syst. Sci., 5905--5915, https://doi.org/10.5194/hess-25-5905-2021, 2021.

Gendron, P.-O., Avaltroni, F., and Wilkinson, K. J.: Diffusion Coefficients of Several Rhodamine Derivatives as Determined by Pulsed Field Gradient–Nuclear Magnetic Resonance and Fluorescence Correlation Spectroscopy, J Fluoresc, 18, 1093–1101, https://doi.org/10.1007/s10895-008-0357-7, 2008.

Ghaderi Zefreh, M., Nilsen, H. M., Lie, K. A., Raynaud, X., and Doster, F.: Streamline simulation of a reactive advective flow with discontinuous flux function, Comput Geosci, 23, 255–271, https://doi.org/10.1007/s10596-018-9771-3, 2019.

Goldberg-Yehuda, N., Assouline, S., Mau, Y., and Nachshon, U.: Compaction effects on evaporation and salt precipitation in drying porous media, Hydrology and Earth System Sciences, 26, 2499–2517, https://doi.org/10.5194/hess-26-2499-2022, 2022.

Guadagnini, A., Sanchez-Vila, X., Saaltink, M. W., Bussini, M., and Berkowitz, B.: Application of a mixing-ratios based formulation to model mixing-driven dissolution experiments, Advances in Water Resources, 32, 756–766, https://doi.org/10.1016/j.advwatres.2008.07.005, 2009.

Hassanali, A., Prakash, M. K., Eshet, H., and Parrinello, M.: On the recombination of hydronium and hydroxide ions in water, Proceedings of the National Academy of Sciences, 108, 20410–20415, https://doi.org/10.1073/pnas.1112486108, 2011.

Himmelsbach, T., Hotzl, H., and Maloszewski, P.: Solute transport processes in a highly permeable fault zone of Lindau fractured rock test site (Germany), Ground Water, 36, 792–800, 1998.

Holzbecher, E.: 12 - REACTIVE TRANSPORT IN POROUS MEDIA—CONCEPTS AND NUMERICAL APPROACHES, in: Transport Phenomena in Porous Media III, edited by: Ingham, D. B. and Pop, I., Pergamon, Oxford, 305–340, https://doi.org/10.1016/B978-008044490-1/50016-8, 2005.

Katz, G. E., Berkowitz, B., Guadagnini, A., and Saaltink, M. W.: Experimental and modeling investigation of multicomponent reactive transport in porous media, Journal of Contaminant Hydrology, 120–121, 27–44, https://doi.org/10.1016/j.jconhyd.2009.11.002, 2011.

Lai, P., Moulton, K., and Krevor, S.: Pore-scale heterogeneity in the mineral distribution and reactive surface area of porous rocks, Chemical Geology, 411, 260–273, https://doi.org/10.1016/j.chemgeo.2015.07.010, 2015.

Li, L., Peters, C. A., and Celia, M. A.: Upscaling geochemical reaction rates using pore-scale network modeling, Advances in Water Resources, 29, 1351–1370, https://doi.org/10.1016/j.advwatres.2005.10.011, 2006.

Li, L., Peters, C. A., and Celia, M. A.: Reply to “Comment on upscaling geochemical reaction rates using pore-scale network modeling” by Peter C. Lichtner and Qinjun Kang, Advances in Water Resources, 30, 691–695, https://doi.org/10.1016/j.advwatres.2006.05.002, 2007.

Lichtner, P. C.: Continuum formulation of multicomponent-multiphase reactive transport, Rev. Mineral., 34, 779–800, 1996.

https://doi.org/10.5194/egusphere-2024-797
Preprint. Discussion started: 2 April 2024

Lichtner, P. C. and Kang, Q.: Comment on: "Upscaling geochemical reaction rates using pore-scale network modeling" by Li, Peters and Celia, Advances in Water Resources, 30, 686–690, https://doi.org/10.1016/j.advwatres.2006.05.005, 2007.

Neina, D.: The Role of Soil pH in Plant Nutrition and Soil Remediation, Applied and Environmental Soil Science, 2019, e5794869, https://doi.org/10.1155/2019/5794869, 2019.

Nissan, A. and Berkowitz, B.: Reactive Transport in Heterogeneous Porous Media Under Different Péclet Numbers, Water Resources Research, 55, https://doi.org/10.1029/2019WR025585, 2019.

Noiriel, C. and Soulaine, C.: Pore-Scale Imaging and Modelling of Reactive Flow in Evolving Porous Media: Tracking the Dynamics of the Fluid–Rock Interface, Transp Porous Med, 140, 181–213, https://doi.org/10.1007/s11242-021-01613-2, 2021.

Nützmann, G., Viotti, P., and Aagaard, P. (Eds.): Reactive transport in soil and groundwater: processes and models, Springer, Berlin, 295 pp., 2005.

Parkhurst, D. L. and Appelo, C. A. J.: PHREEQC (Version 2)-A Computer Program for Speciation, Batch-Reaction, One-Dimensional Transport, and Inverse Geochemical Calculations (Denver, Colorado, USA, US Geological Survey, Water Resources Division), 2013.

Penn, C. J. and Camberato, J. J.: A Critical Review on Soil Chemical Processes that Control How Soil pH Affects Phosphorus Availability to Plants, Agriculture, 9, 120, https://doi.org/10.3390/agriculture9060120, 2019.

Rücker, M.: New Atomic Force Microscopy based analysis tools for investigation of multiphase flow and reactive transport in porous media, n.d.

Shavelzon, E. and Edery, Y.: Shannon Entropy of Transport Self-Organization Due to Dissolution/Precipitation Reaction at Varying Peclet Number in an Initially Homogeneous Porous Media, Hydrology and Earth System Sciences Discussions, 1–35, https://doi.org/10.5194/hess-2023-84, 2023.

Sparks, D. L., Singh, B., and Siebecker, M. G.: Chapter 3 - Chemistry of Soil Organic Matter, in: Environmental Soil Chemistry (Third Edition), edited by: Sparks, D. L., Singh, B., and Siebecker, M. G., Academic Press, Boston, 105–167, https://doi.org/10.1016/B978-0-443-14034-1.00003-4, 2024.

Sposito, G.: The Chemistry of Soils, Oxford University Press, USA, 342 pp., 2008.

Steefel, C. I. and MacQuarrie, K. T. B.: Chapter 2. APPROACHES TO MODELING OF REACTIVE TRANSPORT IN POROUS MEDIA, in: Reactive Transport in Porous Media, edited by: Lichtner, P. C., Steefel, C. I., and Oelkers, E. H., De Gruyter, 83–130, https://doi.org/10.1515/9781501509797-005, 1996.

Stocks-Fischer, S., Galinat, J. K., and Bang, S. S.: Microbiological precipitation of CaCO3, Soil Biology and Biochemistry, 31, 1563–1571, https://doi.org/10.1016/S0038-0717(99)00082-6, 1999.

Stolze, L., Battistel, M., and Rolle, M.: Oxidative Dissolution of Arsenic-Bearing Sulfide Minerals in Groundwater: Impact of Hydrochemical and Hydrodynamic Conditions on Arsenic Release and Surface Evolution, Environmental Science and Technology, 56, 5049–5061, https://doi.org/10.1021/acs.est.2c00309, 2022.

Tartakovsky, A. M., Eichler West, R. M., Scheibe, T. D., and Meakin, P.: Simulations of reactive transport and precipitation with smoothed particle hydrodynamics, J. Comp. Phys., 222, 654–672, doi:10.1016/j.jcp.2006.08.013, 2007.

https://doi.org/10.5194/egusphere-2024-797
Preprint. Discussion started: 2 April 2024

Tartakovsky, A. M., Redden, G., Lichtner, P. C., Scheibe, T. D., and Meakin, P.: Mixing-induced precipitation: Experimental study and multi scale numerical analysis, Water Resour. Res., 44, doi:10.1029/2006WR005725, 2008.

Tartakovsky, A. M., Tartakovsky, G. D., and Scheibe, T. D.: Effects of incomplete mixing on multicomponent reactive transport, Advances in Water Resources, 32, 1674–1679, 2009.

Thabet, K., Le Gal La Salle, A., Quarez, E., and Joubert, O.: Chapter 4 - Protonic-based ceramics for fuel cells and electrolyzers, in: Solid Oxide-Based Electrochemical Devices, edited by: Lo Faro, M., Academic Press, 91–122, https://doi.org/10.1016/B978-0-12-818285-7.00004-6, 2020.

Thullner, M., Van Cappellen, P., and Regnier, P.: Modeling the impact of microbial activity on redox dynamics in porous media, Geochimica et Cosmochimica Acta, 69, 5005–5019, https://doi.org/10.1016/j.gca.2005.04.026, 2005.

Tuckerman, M. E., Chandra, A., and Marx, D.: Structure and Dynamics of OH-(aq), Acc. Chem. Res., 39, 151–158, https://doi.org/10.1021/ar040207n, 2006.

Valocchi, A. J., Bolster, D., and Werth, C. J.: Mixing-Limited Reactions in Porous Media, Transp Porous Med, 130, 157–182, https://doi.org/10.1007/s11242-018-1204-1, 2019.

Varcoe, J. R., Atanassov, P., Dekel, D. R., Herring, A. M., Hickner, M. A., Kohl, P. A., Kucernak, A. R., Mustain, W. E., Nijmeijer, K., and Scott, K.: Anion-exchange membranes in electrochemical energy systems, Energy & environmental science, 7, 3135–3191, 2014.

Waisbord, N. and Guasto, J. S.: Bacterial accumulation in viscosity gradients, in: Am. Phys. Soc. - Div. Fluid Dyn. Meet., Portland, OR, 2016.

Ward, B. B., Arp, D. J., and Klotz, M. G.: Nitrification, American Society for Microbiology Press, 654 pp., 2011.

Wolke, C. T., Fournier, J. A., Dzugan, L. C., Fagiani, M. R., Odbadrakh, T. T., Knorke, H., Jordan, K. D., McCoy, A. B., Asmis, K. R., and Johnson, M. A.: Spectroscopic snapshots of the proton-transfer mechanism in water, Science, 354, 1131–1135, https://doi.org/10.1126/science.aaf8425, 2016.

Zhang, G., Yang, G., Li, S., Shen, Q., Wang, H., Li, Z., Zhou, Y., and Ye, W.: Effects of Hydration and Temperature on the Microstructure and Transport Properties of Nafion Polyelectrolyte Membrane: A Molecular Dynamics Simulation, Membranes, 11, 695, https://doi.org/10.3390/membranes11090695, 2021.